Journal of Radioanalytical and Nuclear Chemistry (2023) 332:4535–4540
https://doi.org/10.1007/s10967-023-09153-3

Surface contaminants' incorporation after nanosecond laser ablation

Wagner Stipp[1,2] · Nathanael Wagner Sales Morais[1] · José Vinicius Martins[3] · Priscila Matos[1] · Jesualdo Luiz Rossi[1] · Wagner de Rossi[1] · Marcus Paulo Raele[1]

Received: 4 August 2023 / Accepted: 6 September 2023 / Published online: 29 September 2023

Abstract

Decontamination and cleaning of surface-contaminated radioactive waste using laser ablation is a promising new technique being researched. One advantage is the potential to recycle waste and reduce the demand for repository storage. However, prior studies have shown that residual radioactivity can persist after laser decontamination indicating the incorporation of contaminants beneath the surface of metal samples. In this study, a q-switched laser was used to measure the depth of the recast zone at various fluences and simulate a decontamination process using a gold-coated sample. The results showed that surface material was found in the recast zone for fluences ranging from 1 to 10 J/cm^2. This suggests that incorporation of surface contaminants after laser ablation is an important issue that must be considered before using this technique for radioactive waste treatment.

Keywords Decontamination · Laser ablation · Radioactive waste · Laser cleaning

Introduction

Surface contaminated radioactive waste (SCRAW) refers to waste that has been contaminated with radioactive materials on its surface. This type of waste typically comes from activities that use or produce radioisotopes, such as nuclear power plants, medical facilities, and laboratories. SCRAWS typically accounts for a significant volume of radioactive waste (95% of the total [1]), and frequently it could be recycled or reuse.

The use of lasers to treat surface contaminated radioactive waste is an emerging technology that has shown promising results [2–10]. The process works by a process known as "laser ablation" [11] in which a pulsed laser (usually nanosecond duration) promotes the evaporation/sublimation of the substrate that contains the contaminant. The vapors/aerosols released [12] can then be captured [12, 13] and safely disposed of, while the material or object is left clean and uncontaminated. The volume that needs to be safeguarded can drastically reduce.

Other benefits of laser decontamination include the ability to decontaminate irregular shapes and difficult to reach surfaces, as well as the potential for reducing waste volumes and exposure to workers during the decontamination process.

When working with metals, which constitute a significant proportion of SCRAWs, the interaction between the laser and the material can be explained as follows: The surface of the metal absorbs the energy from the laser pulse in the irradiated region, causing the temperature to rise to high levels. This heat then propagates to the inner regions, resulting in the formation of a puddle of melted material which eventually evaporates. In certain cases, the melted material can reach temperatures well above its boiling point, leading to the creation of a superheated melt. This leads to the formation of vapor in the superheated melt through homogeneous nucleation, which then rapidly expands, carrying vapor/droplets away from the surface, creating a phenomenon known as phase explosion. In any case, the removal of material from the metal surface by the laser is known as laser ablation.

✉ Marcus Paulo Raele
mpraele@ipen.br

1 Nuclear and Energy Research Institute, IPEN-CNEN/SP, Av. Prof. Lineu Prestes, 2242 - Cidade Universitária, São Paulo, SP, Brasil

2 Federal Institute of Education, Science and Technology of São Paulo, IFSP, Rua Primeiro de Maio 500. Itaquaquecetuba, São Paulo, SP, Brazil

3 Geosciences Institute, University of Sao Paulo, Rua Do Lago, 562 - Cidade Universitária, São Paulo, SP, Brasil

A recent study [14] performed by our research group showed that higher laser intensities (or fluences), depending on the metal, could lead to poorer decontamination. What we actually observed was a resilient residual contamination that did not decrease after successive laser irradiations.

The temperature gradient created by the laser in the melted puddle can result in differences in density across the material, consequently promoting convective currents. Additionally, the Marangoni effect, caused by the surface tension gradient arising from the temperature gradient, can also play a role in creating or contributing to these convective currents. Several studies have numerically simulated these effects, as seen in reference [15–17].

These currents could carry residual contaminants to inner samples regions, which could explain the behavior of the Fig. 1. For higher fluences the gradients could become higher and the currents stronger.

It is worth mentioning that the concentration of low and medium activity levels of SCRAWs is generally in parts per million or billion, which can make assessing these contaminants with spatial resolution a difficult task. However, it is possible to simulate the incorporation process with a higher concentration of a harmless element.

The aim of this study is to confirm the incorporation of surface material into the bulk material due to the laser ablation decontamination.

Material and methods

The ASTM A36 alloy was selected as a substrate due to the formation of a clear boundary of recast material after laser ablation (see Supplementary material Section 1). Thus, allowing the measuring of the melted puddle depth after laser irradiation.

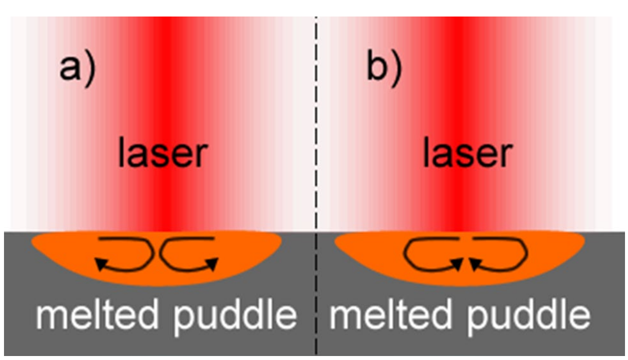

Fig. 1 Unscaled representation of convective currents induced in a melted puddle, which could carry surface contaminants beneath the surface. Flow direction will depend on the material properties, **a** and **b** represents the two possibilities

For the present experiment, we utilized a Q-Switched Nd:YAG laser (Quantel, Ultra 100) with a 7 ns pulse duration and a 20 Hz repetition rate, operating at 1064 nm. The setup included two motorized translation stages (Thorlabs, LTS300/m) in an *XY* configuration to move a vacuum-operated sample holder. A focusing lens (Thorlabs, LA1986) with an effective focal length (EFL) of 125 mm was installed in a manual linear stage to compensate for different sample thicknesses. Figure 2 depicts a schematic of the experimental setup. The beam diameter at the sample surface position was measured using the Kapton® method, with a diameter was 590 µm.

Samples were irradiated accordingly Fig. 3, fluences used were 10, 7.5, 5, 2.5 and 1 J/cm^2. The overlap between consecutive pulses was set at 50% of the damaged area, which was previously measured by an optical microscope. After the irradiation, samples were cut transversely to the irradiation paths, accordingly Fig. 3. One half was embedded in Bakelite, polished, and subjected to etching with a 5% volume solution of nitric acid in ethyl alcohol to expose the crystalline grains (see Supplementary material for more details). The resulting sample is depicted in Fig. 3 (right).

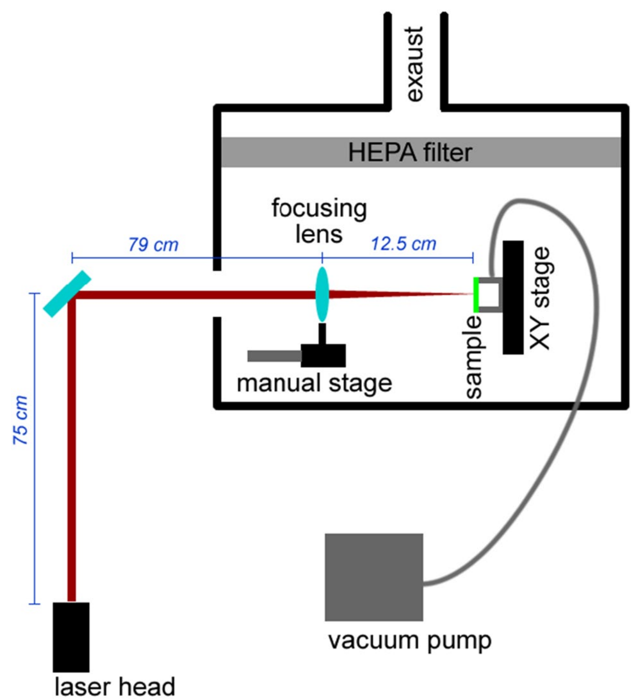

Fig. 2 The experimental setup is schematically illustrated in the figure. To prevent any contact with the sample borders and avoid the use of adhesives or mechanical devices, a vacuum pump was employed to hold the sample in place. The manual stage was adjusted to compensate for variations in sample thickness, ensuring that the focal condition was maintained

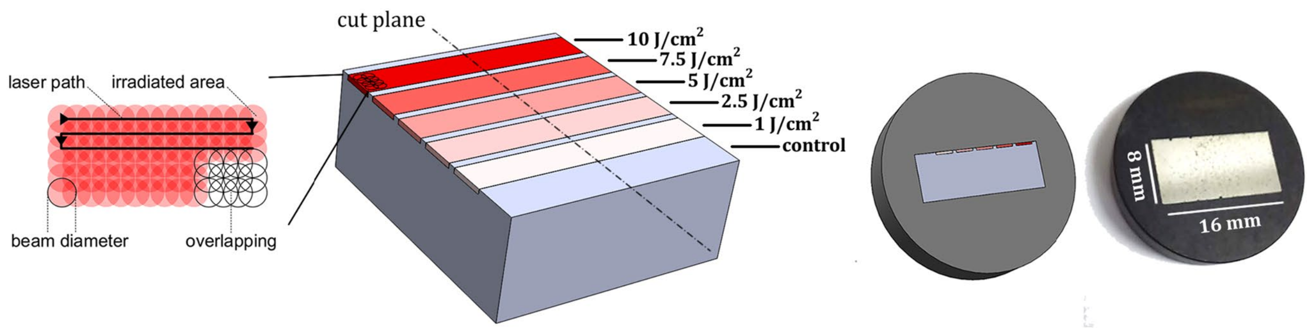

Fig. 3 The applied methodology is illustrated in a schematic diagram, showing a raster pattern with 50% overlapping of the damaged area on the left side. On the right side, different irradiation conditions are depicted, along with the plane where the sample was subsequently cut. Illustration of the final sample, and a photograph of the sample

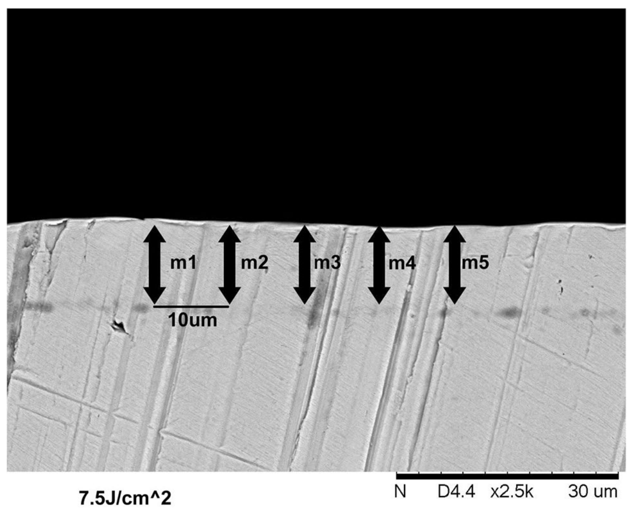

Fig. 4 Representative SEM image and measurement procedure. The sample depicted was irradiated with 7.5 J/cm^2

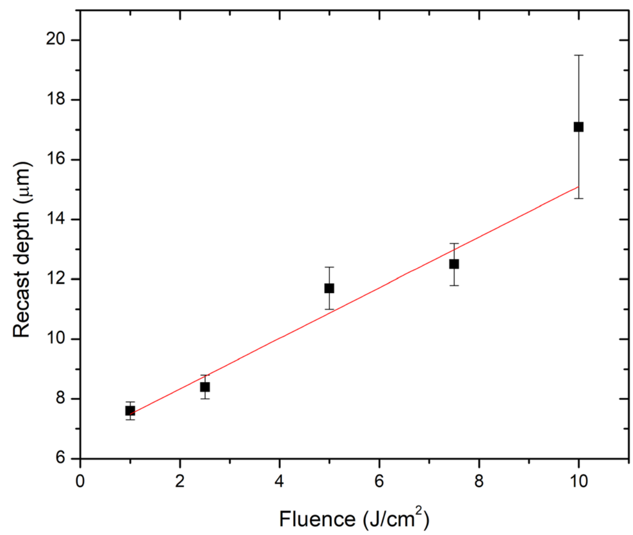

Fig. 5 Recast depth in function of the irradiation fluence, fitting coefficients: slope 0.85 µm/J cm^2 and intercept 6.64 µm (reduced $\chi^2 = 0.93$)

Samples' morphology were analyzed using, optical microscopy, scanning electron microscopy—SEM—(Hitachi 3000).

For elemental analysis a laser ablation induced coupled plasma mass spectrometry—LA-ICP-MS—(Thermo Scientific iCAP Q and CETAC LSX-213 G2+) with a laser spot diameter of 30 µm and fluence of 10.4 J/cm^2 was used.

Results and discussion

First step was to measure the fused layer depth for various irradiation fluences. The eventual recontamination can only occur if the substrate reaches melting temperature, which could promote convective currents. To obtain a statistical variation, sample measurements were taken using SEM images at five different locations, each separated by a distance of 10 µm, Fig. 4.

Even for 1 J/cm^2 recast zone was observed. For the fluence range applied a linear behavior can be associated (Fig. 5).

To investigate the migration of material from the surface to the recast region, a second round of experiments was performed. A similar sample was then cleaned in an ultrasonic bath followed by acetone, and subsequently coated with a 400 nm-thick gold film using a coating system (Leica ACE 200), see Fig. 6 left. The coated sample was then irradiated using the same procedure and subjected to the same methodology of cutting, embedding and polishing as before (Fig. 6, right).

Sampling was conducted to assess the presence of gold beneath the surface using the LA-ICP-MS. To distinguish the contamination profile, sampling was conducted by taking measurements in 3 µm steps (d parameter) starting from the surface and proceeding towards deeper regions,

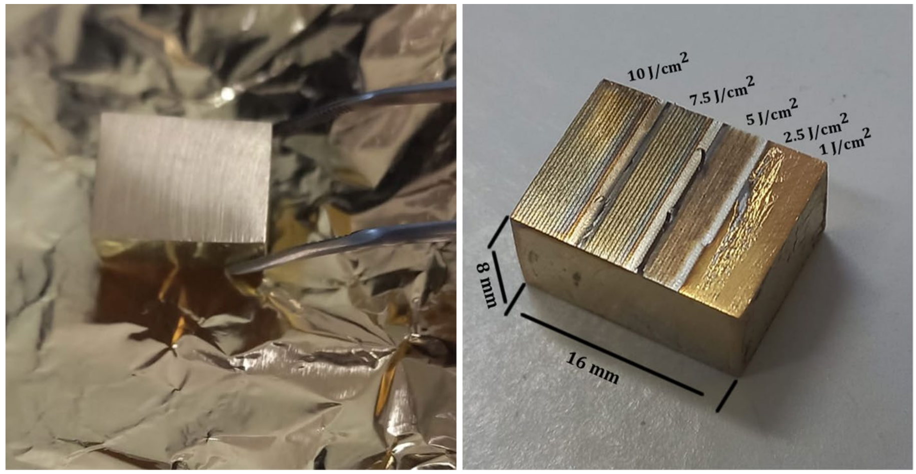

Fig. 6 Sample after the gold coating process (left) and after the laser irradiations (right)

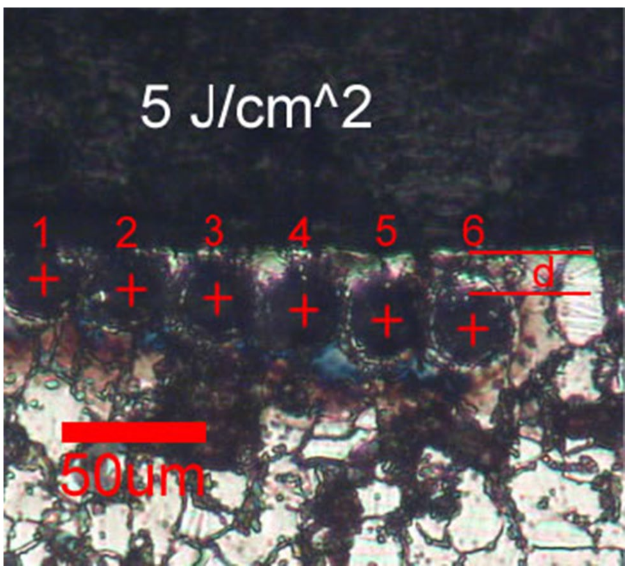

Fig. 7 Representative laser ablated regions by the ICP-MS analysis. Parameter "*d*" is the gap between the surface and the sampling area

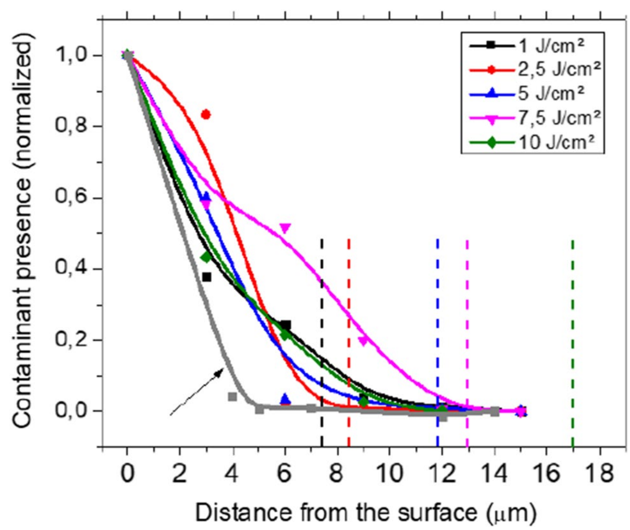

Fig. 8 ICP-MS counts (normalized), in function of the "*d*" gap. A spline curve was added in order to represent the behavior of the incorporation. The dashed lines represent the measured recast zone (Fig. 5)

as shown in Fig. 7, for each spot, 300 laser pulses were shot.

Since statistical variation was not considered, counts were normalized to enable comparisons of behavior between different fluences. Figure 8 shows a plot of "gold presence" as a function of the *"d*" gap (shown in Fig. 7), which indicates the incorporation of gold across all fluences.

The presence of gold beneath the surface was detected in all conditions, pointing the unwanted incorporation of surface material.

At last, a sample containing radioactive material has been generated. This was accomplished by employing a solution containing ^{241}Am, which was subsequently utilized for electrodepositing in a circular area with a diameter of 10 mm (Fig. 9). The resulting activity, as measured with a Beta-Gamma counter (Ludlum, Model 2929, using sensor model 43-10-1), yielded a count of 5840 counts per minute, which is approximately equivalent to 100 Bq.

Next, the sample underwent laser ablation with a fluence of 10 J/cm^2, and the residual activity of alpha particles was evaluated. To further analyze the sample, a sanding process was carried out using 600 grit wet sandpaper. The thickness of the removed material was measured with an optical profilometer, referring to a step height like a machined recess ("*d*" parameter). This iterative process was repeated until reaching the measured recast zone, as indicated in the previous results of this study.

The results were plotted also in Fig. 8, gray line, showing accordance between the data gathered by different approaches.

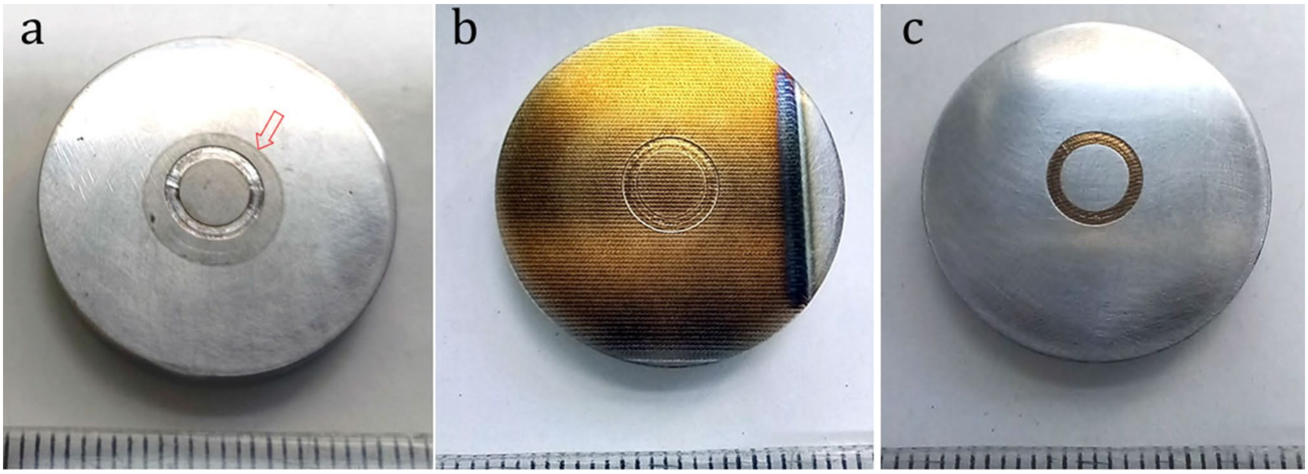

Fig. 9 Sample contaminated in the central area (darker gray stain, pointed out by the red arrow at "**a**"); In **b** irradiated sample, and **c** sanded (representative photograph)

Conclusions

Although laser decontamination is gaining momentum as a promising tool for treating SCRAWs [10], it is important to note that decontamination/cleaning by ablation can sometimes lead to the incorporation of contaminants beneath the surface. This can immobilize the contaminants and hinder further removal, which can be a particular problem in the case of radioactive materials. In some cases, the remaining contamination may be small enough to meet regulatory requirements for regular disposal. However, in other cases, the incorporation of contaminant material may pose undesired destiny to the piece.

The data indicates that, regardless of the irradiation fluence, the penetration of such material was similar for the range and conditions applied. This suggests that the migration range may be related to the solidification time, which is influenced by factors such as the thermal conductivity of the metal. Another hypothesis that was considered is that the convective currents are induced only to a certain depth, regardless of the depth of the melted puddle.

The results are apparently not completely in accordance with the reported results showed in reference [14], since there was not observed incorporation on lower fluences, however, as in this work quantification of the incorporated material between irradiation conditions was not performed, thus this still is an open subject for future studies.

A conservative approach for laser decontamination could involve starting with sub-ablative conditions where the laser is used to induce shockwaves [18] to release loosely attached particles, without generating molten material and avoiding the incorporation of contaminants. After this initial cleaning step, the fluence can be gradually increased to the ablation regime to remove more stubborn contaminants. This approach could potentially minimize the risk of incorporation of contaminants while still achieving effective decontamination.

Supplementary Information The online version contains supplementary material available at https://doi.org/10.1007/s10967-023-09153-3.

Acknowledgements The authors acknowledge the support given by the Brazilian National Council for Scientific and Technological Development—CNPq, grants INFO 465763/2014-6, 422484/2016-4 and Sisfóton 440228/2021-2. We also thank the support given by the Center for Lasers and Applications' Multiuser Facility at IPEN-CNEN/SP and the Support in LA-ICP-MS analysis: Geoanalítica-USP Core Facility (IGc-USP).

Declarations

Conflict of interest The authors declare no conflict of interest. The funders had no role in the design of the study; in the collection, analyses, or interpretation of data; in the writing of the manuscript; or in the decision to publish the results.

References

1. IAEA NW. New IAEA report presents global overview of adioactive waste and spent fuel management. https://www.iaea.org/newscenter/news/new-iaea-report-presents-global-overview-of-radioactive-waste-and-spent-fuel-management.
2. Anthofer A, Lippmann W, Hurtado A (2013) Development and testing of a laser-based decontamination system. Opt Laser Technol 48:589–598
3. Baigalmaa B, Won HJ, Moon JK, Jung CH, Hyun JH (2009) A comprehensive study on the laser decontamination of surfaces contaminated with Cs(+) ion. Appl Radiat Isot 67:1526–1529
4. Delaporte P, Gastaud M, Marine W, Sentis M, Uteza O, Thouvenot P, Alcaraz JL, Le Samedy JM, Blin D (2003) Dry excimer laser cleaning applied to nuclear decontamination. Appl Surf Sci 208:298–305

5. Greifzu G, Kahl T, Herrmann M, Lippmann W, Hurtado A (2019) Laser-based decontamination of metal surfaces. Opt Laser Technol 117:293–298
6. Potiens Jr A, Dellamano J, Vicente R, Raele M, Wetter Z, Landulfo E (2013) Laser decontamination of the radioactive lightning rods. Radiation Phys Chem.
7. Slipchenko NN et al (1999) Application of laser technology for decontamination of steels and alloys used in nuclear power industry. In: Sarkisov AA, du Clos AT (eds) Analysis of risks associated with nuclear submarine decommissioning, dismantling and disposal. NATO science series, vol 24. Springer, Dordrecht. https://doi.org/10.1007/978-94-011-4595-4_42
8. Veiko VP, Mutin TY, Smirnov VN, Shakhno EA (2011) Laser decontamination of radioactive nuclides polluted surfaces. Laser Phys 21:608–613
9. Won H, Park J, Jung C, Choi W, Moon J (2013) Decontamination of radioactive material by Nd:YAG laser. Asian J Chem 25:5819–5822
10. Wang Q, Wang FS, Cai C, Chen H, Ji F, Yong C, Liao DS (2023) Laser decontamination for radioactive contaminated metal surface: a review. Nucl Eng Technol 55:12–24
11. von der Linde D, Sokolowski-Tinten K (2000) The physical mechanisms of short-pulse laser ablation. Appl Surf Sci 154:1–10
12. Herrmann M, Lippmann W, Hurtado A, Asme (2009) The release of radionuclides in the laser decontamination process. Icone 175:211–216.
13. Judson AGBaBF (1955) Filtration of radioactive aerosols by glass fibers. Air Repair 4:223–229.
14. Costa P, Vicente R, Genezini FA, de Rossi W, Raele MP (2022) Laser decontamination of surface impregnated with radioactive material. J Radioanal Nucl Chem 331:4553–4561
15. Yan ZX, Mei XS, Wang WJ, Pan AF, Lin QY, Huang CC (2019) "Numerical simulation on nanosecond laser ablation of titanium considering plasma shield and evaporation-affected surface thermocapillary convection. Opt Commun 453.
16. Liu S, Tian ZJ, Shen LD, Qiu MB (2020) Numerical simulation and experimental investigation of laser ablation of Al2O3 ceramic coating. Materials 13.
17. Guo LY, Geng SN, Gao XS, Wang MW (2021) Numerical simulation of heat transfer and fluid flow during nanosecond pulsed laser processing of Fe78Si9B13 amorphous alloys. Int J Heat Mass Transfer, 170.
18. Zhu GD, Xu ZH, Jin Y, Chen X, Yang LJ, Xu J, Shan DB, Chen YB, Guo B (2022) Mechanism and application of laser cleaning: a review. Opt Lasers Eng, 157.